Ultrapermeable, Reverse-Selective Nanocomposite Membranes

T. C. Merkel,[1] B. D. Freeman,[2] R. J. Spontak,[3] Z. He,[4] I. Pinnau,[4] P. Meakin,[5] A. J. Hill[5]

Polymer nanocomposites continue to receive tremendous attention for application in areas such as microelectronics, organic batteries, optics, and catalysis. We have discovered that physical dispersion of nonporous, nanoscale, fumed silica particles in glassy amorphous poly(4-methyl-2-pentyne) simultaneously and surprisingly enhances both membrane permeability and selectivity for large organic molecules over small permanent gases. These highly unusual property enhancements, in contrast to results obtained in conventional filled polymer systems, reflect fumed silica–induced disruption of polymer chain packing and an accompanying subtle increase in the size of free volume elements through which molecular transport occurs, as discerned by positron annihilation lifetime spectroscopy. Such nanoscale hybridization represents an innovative means to tune the separation properties of glassy polymeric media through systematic manipulation of molecular packing.

Organic-inorganic polymer nanocomposites have attracted wide interest, because the addition of inorganic particles to polymers can enhance conductivity (*1*, *2*), mechanical toughness (*3*), optical activity (*4*, *5*), and catalytic activity (*6*, *7*). Nanocomposites may also prove to be useful for molecular separations, a diverse field affecting processes such as biomolecule purification, environmental remediation, seawater desalination, and petroleum chemicals and fuel production (*8*). These separations are typically accomplished with established technologies such as distillation, absorption, and adsorption, which are often extremely energy- and capital-intensive, or recently by selective permeation through membranes (*8*). Membranes are attractive because they are a low-cost, energy-efficient, green technology. Their widespread use in gas separations has, however, been limited by the difficulty of preparing membranes with the desirable combination of high selectivity, which yields high product purity and low operating costs, and high permeability, which reduces membrane area and capital cost. Unfortunately, as the selectivity of conventional polymer membrane materials increases, permeability invariably decreases and vice versa (*9*, *10*). Attempts (*11*–*13*) to overcome this fundamental limitation have explored the addition of micron-sized porous zeolite particles to organic polymers in the hope of combining the mechanical elasticity and processability of polymers with the strong size selectivity characteristic of spatially well-defined zeolite pores. Commercialization of this approach, however, has been hampered by poor polymer/zeolite adhesion and inadequate particle dispersion (*13*).

Conventional, or size-selective, polymer membranes preferentially allow small molecules (such as H_2) to permeate relative to larger ones (such as methane). However, another class of membranes, reverse-selective membranes, preferentially allows larger species to permeate in a mixture. This counterintuitive property is possible because molecular transport in dense polymer membranes is governed by both penetrant solubility and diffusivity (*14*). The permeability P of such a membrane may be expressed as $P = S \times D$, where S and D are the penetrant solubility and diffusion coefficients, respectively. The selectivity of a membrane for component A over component B, $\alpha_{A/B}$, is

$$\alpha_{A/B} = \left(\frac{S_A}{S_B}\right) \times \left(\frac{D_A}{D_B}\right) \quad (1)$$

where the first term on the right-hand side is the solubility selectivity and the second is the diffusion selectivity. Generally speaking, as penetrant size increases, solubility often increases while the diffusion coefficient usually decreases (*15*). Polymers with a very flexible chain backbone or rigid ones that pack poorly and exhibit very high free volume sieve molecules poorly based on differences in size. Consequently, it is possible to prepare membranes from such materials having sufficiently weak diffusion selectivity (that is, $D_A/D_B \rightarrow 1$) so that larger, more soluble vapors (such as *n*-butane) permeate more easily than light gases (such as H_2). These reverse-selective membranes are useful in industrial separations in which the smaller, less soluble gas component in a mixture is required at high pressure because it is the larger molecules that preferentially pass through to the low-pressure side. Examples of reverse-selective membrane applications include the removal of higher hydrocarbons from methane in the purification of natural gas, organic monomer separation from nitrogen in the production of polyolefins, and hydrocarbon removal from hydrogen in refinery applications (*15*). Reverse-selective membranes are not subject to the permeability/selectivity tradeoff inherent in conventional size-selective polymer membranes; more permeable reverse-selective membranes tend to be more selective (*15*). Polymers exhibiting the most favorable reverse selectivities and highest permeabilities are high–glass transition temperature, amorphous, high-free-volume (that is, low-density) substituted polyacetylenes, such as poly(4-methyl-2-pentyne) (PMP) (*16*). The addition of nanoscale inorganic particles to such existing polymers offers a new and unexplored route to tune the molecular parameters governing membrane selectivity (*17*).

Molecular transport through a dense polymer depends strongly on the amount of free volume, or space not occupied by polymer chains, in the material (*18*). Free volume, whether static voids created by inefficient chain packing or transient gaps generated by thermally induced chain segment rearrangement, presents diffusing molecules with a low-resistance avenue for transport. The larger and more numerous these pathways are, the faster molecules migrate through a polymer. These free volume considerations are embodied in the following statistical mechanics model of Cohen and Turnbull (*19*)

$$D_A = \alpha \exp(-\gamma v_A / V_{FV}) \quad (2)$$

where α and γ are positive constants, v_A is the minimum volume required for penetrant A to execute a diffusion step and hence is a measure of penetrant size, and V_{FV} is the average polymer free volume. Insertion of Eq. 2 into Eq. 1 reveals that the diffusion selectivity D_A/D_B is proportional to $\exp(\gamma(v_B - v_A)/V_{FV})$ and, when species A is a larger vapor molecule and B is a small gas molecule, approaches 1 as the average polymer free volume increases. That is, increasing polymer free volume enhances reverse selectivity.

Because the reverse-selective nature of PMP is related to its intrinsically high free volume caused by inefficient chain packing (*16*), further disruption of molecular packing

[1]Center for Energy Technology, Research Triangle Institute, Research Triangle Park, NC 27709, USA. [2]Department of Chemical Engineering, Center for Energy and Environmental Resources, University of Texas at Austin, Austin, TX 78758, USA. [3]Department of Chemical Engineering, North Carolina State University, Raleigh, NC 27695, USA. [4]Membrane Technology and Research, Menlo Park, CA 94025, USA. [5]Commonwealth Scientific and Industrial Research Organisation–Division of Manufacturing Science and Technology, Clayton, Victoria 3168 Australia. [6]School of Chemistry, Monash University, Clayton, Victoria, 3800 Australia.

should increase the free volume of PMP and, in turn, its reverse selectivity. We hypothesize that this effect can be realized through the use of fine filler particles as "nanospacers" to prevent rigid PMP chains from packing closely. This speculation, however, is completely contrary to the established principle that adding impermeable filler particles to a polymer leads to a systematic reduction in molecular transport (*20*). In fact, this effect is exploited to enhance barrier properties of polymer films. Numerous models, based on theories of composite materials, have been proposed to describe the reduction in permeability of filled polymers (*20*). One of the most frequently used examples of such models is derived from Maxwell's analysis of the steady-state dielectric properties of a dilute suspension of spheres (*21*)

$$P_c = P_p\left(\frac{1-\phi_f}{1+\frac{\phi_f}{2}}\right) \quad (3)$$

where P_c is the permeability of the composite medium, P_p is the permeability of the pure polymer, and ϕ_f is the volume fraction of filler. The Maxwell equation captures the notion that filler particles obstruct molecular transport and, despite its simplicity, is consistent with transport data in a variety of filled polymer systems (*20*). Physically, reduced permeability in filled polymers is attributed to the increase in diffusion path length and decrease in effective cross-sectional area available for transport as filler concentration increases.

We have mixed PMP with TS-530 fumed silica particles (Cabot Corporation, Tuscola, IL) possessing hydrophobic trimethylsilyl surface groups. The estimated primary particle diameter of these small particles is 13 nm. In contrast to the role of zeolites in filled membranes, nonporous fumed silica particles do not permeate or sieve gas molecules themselves. Rather, the small size of the fumed silica particles is used to alter polymer chain packing and, in turn, permeation and separation properties without introducing gross selectivity-destroying defects at loadings of up to 50 weight % (wt%). In a robust fabrication process, mechanically tough nanocomposite films are prepared by solution casting after physical mixing of fumed silica powder with polymer and cyclohexane. Good dispersion of fumed silica particles in PMP is obtained by matching the polarity of the polymer medium and particle surface groups, as well as by controlling film drying conditions.

The conventional transport behavior established by Eq. 3 and the surprising departure of our filled system from it are demonstrated in Fig. 1. The permeability of PMP to methane, and all other gases tested, systematically increases with increasing fumed silica loading. At 50 wt% fumed silica, the highest filler concentration examined, the PMP/fumed silica nanocomposite permeability is more than 240% greater than that of pure PMP. In sharp contrast, Maxwell's equation predicts a 35% reduction in permeability at the same filler loading. The validity of Maxwell's model for conventional filled systems is highlighted by the data of Barrer *et al.* (*22*), which are included in Fig. 1 for comparison. In traditional filled systems, flexible rubbery polymer chains mix with nanoscale particles without increasing free volume in the polymer phase, resulting in a more tortuous diffusion path, smaller cross-sectional area available for transport, and consequently reduced permeability. Clearly, this is not the dominant effect in rigid glassy PMP, in which the addition of fumed silica increases penetrant transport rates.

In rare cases where filler addition has been shown to increase gas flux through a material, such as in some zeolite-filled polymers, this result has been ascribed to the creation of micron-scale defects at the polymer/filler interface that permit fast but relatively nonselective Knudsen diffusion (*13*). Evidence that this mechanism is not operative in our nanocomposites is presented in Fig. 2. As the fumed silica concentration in PMP increases, *n*-butane permeation and the selectivity of the membrane for *n*-butane over methane increase simultaneously and significantly (*23*). Knudsen flow, and the relatively large pathways associated with this diffusive mechanism, favor methane transport and, if present, would reduce *n*-butane/methane selectivity. Our results are consistent with true molecular mixing of fumed silica and PMP and confirm that the transport properties of a nanocomposite can be tuned while maintaining the defect-free, mechanically strong films necessary for practical implementation (*24*). By disrupting the packing of rigid bulky PMP chains, fumed silica apparently increases accessible free volume in the polymer matrix without introducing cavities large enough to promote weakly selective or nonselective free-phase flow mechanisms (such as Knud-

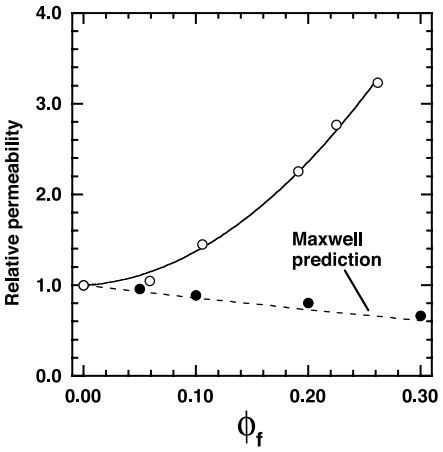

Fig. 1. The ratio of penetrant permeability in the nanocomposite to that in the pure polymer as a function of filler volume fraction. Filler volume fraction is estimated from $\phi_f = m_f/(m_f + m_p\rho_f/\rho_p)$, where *m* and ρ refer to the mass and density, respectively, of filler (f) and polymer (p) used in the nanocomposite. The dashed line represents the Maxwell model prediction (Eq. 3). Our data (open circles) are for methane permeation at 25°C in PMP containing nanoscale fumed silica (TS-530 from Cabot). Included for comparison are the data of Barrer *et al.* (*22*) for propane permeation at 40°C in natural rubber containing ZnO filler (solid circles).

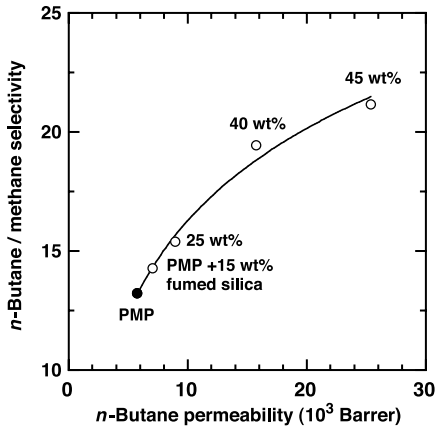

Fig. 2. The effect of fumed silica (TS-530) content on *n*-butane permeability and *n*-butane/methane selectivity of glassy PMP. These data were acquired at 25°C from mixtures composed of 98 mole % methane and 2 mole % *n*-butane at a feed pressure of 11.2 atm and a permeate pressure of 1 atm.

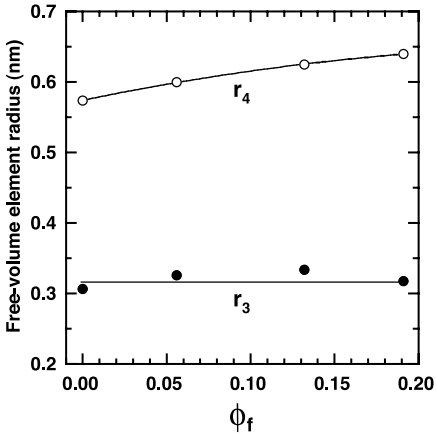

Fig. 3. The concentration dependence of average free-volume element size (r_3 and r_4) in PMP, as ascertained by PALS. Values of r_3 and r_4 are calculated from *o*-Ps lifetimes (τ_3 and τ_4, respectively) according to $1/\tau_i = 2[1 - (r_i/r_0) + (1/2\pi)\sin(2\pi r_i/r_0)]$, which assumes that the *o*-Ps probe is at the core of a spherical void. Here, r_0 denotes the electron layer thickness, estimated to be 0.1656 nm (*18*). The PALS spectra were acquired at ambient temperature in a nitrogen environment and were modeled as the sum of four decaying exponentials with the computer algorithm PFPOSFIT (*18*).

sen or Poiseuille transport). This increase in free volume augments molecular diffusion coefficients and weakens the size-sieving nature of PMP, factors that increase both permeability and reverse selectivity.

A convenient measure of the size and concentration of static and dynamic free volume elements in condensed matter is provided by positron annihilation lifetime spectroscopy (PALS) (*25*). In this technique, a positron is injected into a sample; forms a spin parallel bound state with an electron, which is called ortho-positronium (*o*-Ps); and then annihilates with an antiparallel electron of the surrounding medium to form gamma rays. The lifetime of an *o*-Ps particle depends on the electron density in its local environment, which is sensitive to the size of the free volume element in which it resides. In some very high-free-volume polymers, PALS analysis reveals a bimodal distribution of free volume elements (*18*). In addition to smaller cavities with radii (r_3) of 0.3 to 0.4 nm that are typical of cavities in most polymers, high-free-volume materials, such as PMP, also possess larger free-volume elements with radii (r_4) of 0.5 to 1.0 nm. These large-free-volume cavities have been described as interconnected pathways through which most penetrant transport occurs (*26*). As illustrated in Fig. 3, the addition of fumed silica to PMP systematically increases the average size of these large-free-volume elements. The total increase in free volume radius at high fumed silica loading is less than 0.1 nm, emphasizing the true molecular-scale alteration of PMP chain packing engineered by nanoscale fumed silica. Material modification on this scale may be necessary to manipulate, in controllable fashion, transport characteristics, because penetrant size differences of less than 0.02 nm can yield substantial differences in flux through polymer membranes. For example, in strongly size-sieving polymers, selectivities as high as eight are observed for O_2 relative to N_2, despite a difference of only 0.018 nm in the kinetic diameters of these two gas molecules (*9*).

The importance of using small filler particles to achieve the desired effect on transport in PMP is demonstrated in Fig. 4. In addition to the primary fumed silica filler used in this work, several other silicas of varying size, as well as carbon black and α-alumina powder, have been added to PMP. Although all of these particles demonstrated some ability to enhance the permeability of PMP, at equivalent volume fractions smaller primary particles appear more effective at increasing flux, with significant increases in permeability observed only for particles smaller than 50 nm. From these data we conclude that, for a fixed volume fraction, smaller particles yield more polymer/particle interfacial area and provide more opportunity to disrupt polymer chain packing and affect molecular transport.

The distribution of fumed silica particles in PMP is shown in the transmission electron microscopy (TEM) images presented in Fig. 5. Consistent with the general network-forming properties of fumed silica, some primary particles aggregate into clusters ranging up to a few hundred nanometers in diameter. These clusters possess a highly fractal surface, which together with discrete primary particles yields a large polymer/filler interface. The TEM images reveal that the number of fumed silica particles, as well as their mean aggregate size, increases with fumed silica concentration. Comparison with aggregate sizes discerned from light scattering of dilute fumed silica solutions confirms that these particles are well dispersed in PMP. This result is indicative of weak polymer/filler interactions, which is expected on the basis of matrix polarity and fumed silica surface chemistry. The observed fumed silica dispersion is consistent with our transport data, because highly networked fumed silica would be expected to promote Knudsen diffusion and thereby reduce reverse selectivities.

We have observed similar effects on small molecule transport when fumed silica is added to other high-free-volume glassy polymers, including poly(1-trimethylsilyl-1-propyne) and a copolymer of tetrafluoroethylene and 2,2-bis(trifluoromethyl)-4,5-difluoro-1,3-dioxole, which suggests that this approach may have broad applicability. Although previous efforts (*13*) have sought to harness the selective pores of inorganic zeolite particles dispersed within a polymeric matrix to enhance membrane performance, we have demonstrated that nonporous particles, having dimensions comparable to those of individual polymer chains, can be used to regulate the manner in which these chains pack and thereby favorably manipulate molecular transport and selectivity.

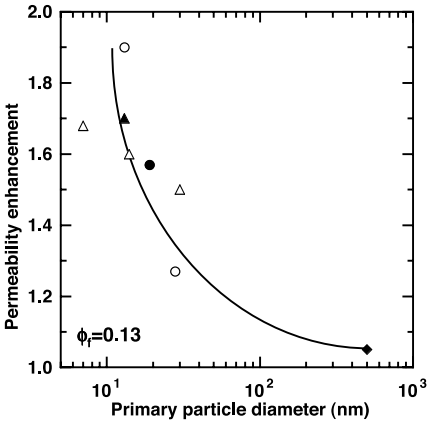

Fig. 4. The effect of filler primary particle size on methane permeability enhancement (that is, the ratio of permeability in filled PMP to that in unfilled PMP) at constant filler concentration [13 volume % (vol%)]. Hydrophobic fumed silicas (Cabot TS-530, 13 nm, with trimethylsilyl surface groups; or TS-720, 27 nm, with polydimethylsiloxane surface groups) are shown as open circles. Hydrophilic fumed silicas with hydroxyl surface groups (Cabot L-90, M-5 and EH-5) are displayed as open triangles. Included for comparison are a precipitated silica (Hi-Sil 233, solid circle) from PPG Industries (Pittsburgh, PA), a high surface-area carbon black (Monarch 1300, solid triangle) from Cabot Corporation and a fine α-alumina (solid diamond) from Research Triangle Institute (Research Triangle Park, NC).

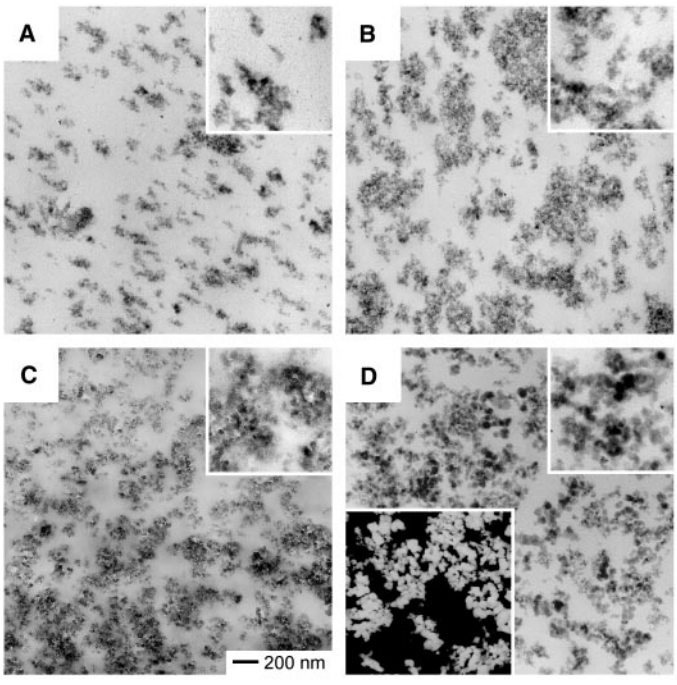

Fig. 5. Energy-filtered TEM images of PMP containing different concentrations (in wt%/vol%) of a hydrophobic fumed silica (TS-530): (**A**) 15/6, (**B**) 30/13, and (**C**) 40/19. The image displayed in (**D**) is obtained from PMP containing a hydrophilic fumed silica (L-90) at the same loading level as in (C), and the matched contrast-inverted image is a Si image confirming that the particles are siliceous. The insets provided in each image correspond to a ×3 increase in magnification. These images have been acquired from thin (~70 nm) microtomed specimens on a Zeiss EM902 electron spectroscopic microscope operated at 80 kV and energy-loss settings of 0 to 270 eV.

References and Notes

1. E. Coronado, J. R. Galan-Mascaros, C. J. Gomez-Garcia, V. Laukhin, *Nature* **408**, 447 (2000).
2. F. Croce, G. B. Appetecchi, L. Persi, B. Scrosati, *Nature* **394**, 456 (1998).
3. T. J. Pinnavaia, *Science* **220**, 365 (1983).
4. Y. Wang, N. Herron, *Science* **273**, 632 (1996).
5. J. G. Winiarz, L. M. Zhang, M. Lal, C. S. Friend, P. N. Prasad, *J. Am. Chem. Soc.* **121**, 5287 (1999).
6. G. Schmid, Ed., *Clusters and Colloids* (Wiley, Weinheim, Germany, 1994).
7. S. N. Sidorov *et al.*, *J. Am. Chem. Soc.* **123**, 10502 (2001).
8. M. B. Shiflett, H. C. Foley, *Science* **285**, 1902 (1999).
9. L. M. Robeson, *J. Membr. Sci.* **62**, 165 (1991).
10. B. D. Freeman, *Macromolecules* **32**, 375 (1999).
11. S. Kulprathipanja, R. W. Neuzil, N. Li, U.S. Patent 4,740,219 (1988).
12. M. Jia, K. V. Peinemann, R. D. Behling, *J. Membr. Sci.* **57**, 289 (1991).
13. R. Mahajan, C. M. Zimmerman, W. J. Koros, in *Polymer Membranes for Gas and Vapor Separation: Chemistry and Materials Science*, B. D. Freeman, I. Pinnau, Eds. (American Chemical Society, Washington, DC, 1999), pp. 277–286.
14. T. Graham, *Philos. Mag.* **32**, 401 (1866).
15. B. D. Freeman, I. Pinnau, *Trends Polym. Sci.* **5**, 167 (1997).
16. A. Morisato, I. Pinnau, *J. Membr. Sci.* **121**, 243 (1996).
17. I. Pinnau, Z. He, U.S. Patent 6,316,684 (2001).
18. V. P. Shantarovich, I. B. Kevdina, Y. P. Yampolskii, A. Y. Alentiev, *Macromolecules* **33**, 7453 (2000).
19. M. H. Cohen, D. Turnbull, *J. Chem. Phys.* **3**1, 1164 (1959).
20. R. M. Barrer, in *Diffusion in Polymers*, J. Crank, G. S. Park, Eds. (Academic Press, New York, 1968), pp. 165–217.
21. C. Maxwell, *Treatise on Electricity and Magnetism* (Oxford Univ. Press, London, 1873), vol. 1.
22. R. M. Barrer, J. A. Barrie, M. G. Rogers, *J. Polym. Sci. Part A* **1**, 2565 (1963).
23. The results presented in Figs. 1 and 2 were highly reproducible. Using a wide variety of gases, we measured the properties of many films as functions of pressure and the number of pressurization and depressurization cycles. Permeability and selectivity did not depend on the number of pressurization and depressurization cycles. Sample-to-sample variability was always within the typical range of experimental uncertainty (±7% for permeability, ±5% solubility, and ±15% for diffusivity).
24. The results in Fig. 2 for films were validated in state-of-the-art thin film composite membranes prepared from mixtures of PMP and fumed silica, and these thin film composite membranes were used to successfully prepare 1-square-meter pilot-scale spiral wound modules.
25. Y. Kobayashi, K. Haraya, S. Hattori, T. Sasuga, *Polymer* **35**, 925 (1994).
26. I. Pinnau, L. G. Toy, *J. Membr. Sci.* **116**, 199 (1996).

27. Funded by NSF (grants DMI-9901788 and CTS-9803225) and the U.S. Department of Energy (grant DE-FG02-99ER14991).

7 January 2002; accepted 12 March 2002

The Cause of Carbon Isotope Minimum Events on Glacial Terminations

Howard J. Spero[1]* and David W. Lea[2]

The occurrence of carbon isotope minima at the beginning of glacial terminations is a common feature of planktic foraminifera carbon isotopic records from the Indo-Pacific, sub-Antarctic, and South Atlantic. We use the $\delta^{13}C$ record of a thermocline-dwelling foraminifera, *Neogloboquadrina dutertrei*, and surface temperature estimates from the eastern equatorial Pacific to demonstrate that the onset of $\delta^{13}C$ minimum events and the initiation of Southern Ocean warming occurred simultaneously. Timing agreement between the marine record and the $\delta^{13}C$ minimum in an Antarctic atmospheric record suggests that the deglacial events were a response to the breakdown of surface water stratification, renewed Circumpolar Deep Water upwelling, and advection of low $\delta^{13}C$ waters to the convergence zone at the sub-Antarctic front. On the basis of age agreement between the absolute $\delta^{13}C$ minimum in surface records and the shift from low to high $\delta^{13}C$ in the deep South Atlantic, we suggest that the $\delta^{13}C$ rise that marks the end of the carbon isotope minima was due to the resumption of North Atlantic Deep Water influence in the Southern Ocean.

A persistent feature of planktic and intermediate-depth benthic foraminifera carbon isotope records from tropical through Southern high latitudes is the large (0.3 to 1.2‰), rapid negative $\delta^{13}C$ excursions that are observed on deglaciations (*1–5*). Because these carbon isotope events occur when the northern hemisphere ice sheets are collapsing, it is difficult to explain them via the transfer of isotopically light carbon from the terrestrial to oceanic carbon reservoirs. Rather, since the terrestrial biosphere was already expanding and sequestering ^{12}C-rich CO_2 into biomass, and the glacial oceans were preconditioned with a low $\delta^{13}C$ signature from remineralized terrestrial carbon during ice sheet growth (*6*), one would expect the $\delta^{13}C$ of the oceanic carbon reservoir to increase at the end of glacials. The extensive distribution of these $\delta^{13}C$ minima in the tropical Indo-Pacific, south Atlantic and sub-Antarctic and the rate at which the full signal appears in different basins, suggests the signal source originates from an oceanic region with direct connection to the different ocean basins (*5*).

Ninnemann and Charles (*5*) argued that these carbon isotope minima could not be a whole ocean signal because they are absent from north Atlantic planktonic records. Rather, they suggested that the tropical Indo-Pacific surface $\delta^{13}C$ minima were due to the transfer of a preformed $\delta^{13}C$ signal from the sub-Antarctic via Antarctic Intermediate Water (AAIW) or sub-Antarctic Mode Water (SAMW) (*2, 7*), with subsequent propagation through the low-latitude thermocline. They further proposed that the signal source was a change in gas exchange fractionation across the air-sea interface as Southern Ocean temperatures warmed at the end of glacials. Because a decrease in $^{13}C/^{12}C$ fractionation would accompany a general postglacial oceanic surface temperature (SST) increase, (*5*) predicted that the $\delta^{13}C$ of atmospheric CO_2 should rise as oceanic $\delta^{13}C$ decreased. However, $\delta^{13}C$ data from Late Quaternary packrat middens (*8*) and CO_2 from the Taylor Dome ice core (*9*) show that atmospheric $\delta^{13}C$ initially decreased as the deglaciation began, and did not begin to increase until ~3 thousand years (ky) later. These atmospheric proxies are not consistent with the proposed equilibration mechanism, requiring us to explore alternatives to explain the termination $\delta^{13}C$ events.

Site TR163-19 is located on the Cocos Ridge in the eastern equatorial Pacific (EEP) (2°15.5′N, 90°57.1′W, 2348 m water depth), just north of the cold upwelling water that characterizes much of this region (*10*). Here, the subsurface thermocline waters are thought to be strongly influenced by sub-Antarctic water masses via the equatorial undercurrent (EUC) (*11, 12*) and the region is not complicated by changes in the position of deep ocean currents with different isotopic composition as is the case in the Atlantic Ocean (*13*). The source of the EUC and waters upwelling from the Peru-Chile undercurrent is likely SAMW, which forms north of the sub-Antarctic front and is the major precursor to AAIW (*14*). It is thought that SAMW ventilates the Pacific Ocean as AAIW by subduction and northward advection into the Pacific subtropical gyre from its primary source in the southeast Pacific (*15*). The dense component of SAMW subsequently flows through the Drake Passage where it is slightly modified, finally becoming the main core of AAIW in the Atlantic and Indian Oceans. In the southwest Pacific, older AAIW flows into the Pacific subtropical gyre where it also contributes to the EUC. The nutrient and $\delta^{13}C$ content of Pacific AAIW is set by the chemistry of upwelled circumpolar deep water (CPDW) and partial equil-

[1]Department of Geology, University of California, Davis, CA 95616, USA. [2]Department of Geological Sciences and the Marine Science Institute, University of California, Santa Barbara, CA 93106, USA.

*To whom correspondence should be addressed. E-mail: spero@geology.ucdavis.edu